FAR-INFRARED OPTICAL PROPERTIES OF THE HEAVY FERMION SUPERCONDUCTOR UBe_{13}

By

Adán Brown

B.Sc. Physics

A THESIS SUBMITTED IN PARTIAL FULFILLMENT OF

THE REQUIREMENTS FOR THE DEGREE OF

MASTER OF SCIENCE

in

THE FACULTY OF MATHEMATICS AND SCIENCE

DEPARTMENT OF PHYSICS

We accept this thesis as conforming

to the required standard

.....

.....

.....

.....

.....

BROCK UNIVERSITY

September, 2001

© Adán Brown, 2001

Acknowledgement

I would like to extend my sincere gratitude to Dr. Maureen Reedyk for her great support and insight throughout these years. Her dedication, effort, and tremendous patience has played a key role in the successful completion of this thesis. I would also like to thank the rest of the faculty for their contribution, not only toward this thesis but also for my undergraduate education. Special thanks to Dr. Razavi and Dr. Mitrovic for their support and encouragement. Some of those harsh, but well deserved words, I will never forget. I like to thank as well Dr. Shukla for his devotion and the numerous conversations we had to further develop my education. I find it important to also thank other people whose efforts underlie every research project done here at the university. I would like to thank the members of the machine and electronic shops, as well as the people in charge of maintaining the liquid nitrogen system. With out them our experiments couldn't have been completed.

Thanks to Dr. Timusk and staff for allowing us to perform experiments and for taking the time to show us the ropes in their laboratory. Also, J. L. Smith at Los Alamos for providing the samples.

A special thanks to my fellow classmates: Tim, Mylo, Sarkis, Rodica, Miro.

The most important people that I wish to thank are my family. My parents, Patricia and Adam, who have helped me, encouraged me, and gave me a place to stay. We have gone through difficult times, for the past 6 years, and together, with a lot of hard work, we have succeeded in establishing ourselves in this new country.

Abstract

Temperature dependent resistivity, ρ, magnetic susceptibility, χ, and far-infrared reflectance measurements were made on the low T_c superconductor UBe_{13}. Two variants of UBe_{13} have been proposed, named 'L'- (for low T_c) and 'H'-type (for high T_c). Low temperature resistivity measurements confirmed that our sample was of H-type and that the transition temperature was at 0.9 K. This was further confirmed with the observation of this transition in the AC-susceptibility. Low temperature reflectance measurements showed a decrease in the reflectivity as the temperature is lowered from 300 to 10 K, which is in qualitative agreement with the increasing resistivity in this temperature range as temperature is lowered. No dramatic change in the reflectivity was observed between 10 and 0.75 K. A further decrease of the reflectance was observed for the temperature of 0.5 K. The calculated optical conductivity shows a broad minimum near 80 cm^{-1} below 45 K. Above 45 K the conductivity is relatively featureless. As the temperature is lowered, the optical conductivity decreases. The frequency dependent scattering rate was found to be flat for temperatures between 300 and 45 K. The development of a peak, at around 70 cm^{-1} was found for temperatures of 45 K and below. This peak has been associated with the energy at which the transition to a coherent state occurs from single impurity scattering in other heavy fermion systems. The frequency dependent mass enhancement coefficient was found to increase at low frequencies as the frequency decreases. Its' magnitude as frequency approaches zero also increased as the temperature decreased.

Table of Contents

Acknowledgement ii

Abstract iii

1 Introduction 1

1.1 Heavy Fermions 1

1.2 UBe_{13} - Previous Studies 4

2 Characterization of UBe_{13} 13

2.1 DC-Resistivity 13

2.1.1 Background 13

2.1.2 Experimental Details 14

2.1.3 Results 15

2.2 AC-Susceptibility 18

2.2.1 Background 18

2.2.2 Experimental Details 19

2.2.3 Results 21

3 Normal and Superconducting State Optical Properties of UBe_{13} 23

3.1 Background 23

3.2 Experimental Details 24

3.2.1 The Martin Puplett type Polarizing Interferometer and the He^3 Cryostat - Brock University 25

3.2.2 Fast Fourier Transform Interferometer - McMaster University. . . 27
3.3 Reflectance of UBe_{13} - Experimental Results 28
3.3.1 Mathematical Analysis using Kramers-Kronig Relations 30
3.4 Optical Conductivity of UBe_{13} - Experimental Results 30
3.5 Frequency Dependent Scattering Rate of UBe_{13} - Experimental Results . 31
3.6 Frequency Dependent Mass Enhancement of UBe_{13} - Experimental Results 33
3.7 Discussion 35
3.7.1 High Temperature Measurements 35
3.7.2 Low Temperature Measurements 38

4 Conclusions **40**
4.1 Remarks 40
4.2 Characterization Results 40
4.3 Optical Properties 41

Appendices **43**

A Reflectivity and Phase Shift **43**

Bibliography **45**

List of Tables

1.1 Ordering in some heavy fermion systems. 2

1.2 Zero-Temperature values of the Specific heat coefficient, γ. 3

1.3 Typical values of the room temperature resistivity of heavy fermions. . . 6

List of Figures

1.1 Specific heat at constant pressure for some heavy fermion systems [1]. . . 4

1.2 Resistivity of several heavy fermion systems [1]. Note that the resistivities at room temperature have been normalized to the same values. 5

1.3 Crystal Structure of UBe_{13}. 7

1.4 Specific heat and Magnetic susceptibility of UBe_{13} [5]. 8

1.5 Specific heat of UBe_{13} 9

1.6 Resistivity of UBe_{13} [5]. 10

1.7 Absorptivity by Bommeli *et. al.* [7]. 10

1.8 Optical Conductivity by Bommeli *et. al.* [7]. 11

1.9 Reflectance measured by Bonn *et. al.* [8]. 11

1.10 Optical conductivity determined by Bonn *et. al.* [8]. 12

2.1 Typical sample configuration for resistivity measurements. 14

2.2 Resistivity of UBe_{13}. Inset shows the transitions. 15

2.3 Resistivity setup on the sample stage of the cryostat. 17

2.4 Resistivity of UBe_{13} mounted on the sample stage. 18

2.5 Diagram of Ac-Susceptometer coils. 19

2.6 Circuit diagram for electronic balancing of secondary coils [14]. 20

2.7 Sample holder for the AC-susceptometer. 21

2.8 Susceptibility of UBe_{13} sample 1909. 22

3.1 Picture of the Brock University Cryostat. 25

3.2 Sample load curve for bias voltage determination [16]. 27

3.3 Reflectance of UBe_{13}. 29
3.4 Real part of the Optical Conductivity of UBe_{13}. Y-axis shows dc-conductivity values taken from Knetsch et. al. [19]. 32
3.5 Frequency dependent Scattering Rate of UBe_{13}. Some calculated dc-values are shown along the y-axis [19]. 33
3.6 Frequency dependent mass enhancement of UBe_{13}. 34
3.7 Resistivity of UBe_{13} with impurities and magnetic field 36
3.8 Temperature and Frequency dependent optical conductivity of the Anderson impurity model[25]. 37
3.9 Frequency dependent Scattering Rate of UBe_{13} (low temperatures). The calculated dc-value at 1 K is shown on the y-axis. 39

Chapter 1

Introduction

The unusual behavior of heavy fermion systems continues to attract both experimental and theoretical attention. Heavy fermion metals are usually described as a new class of metals. These electrically conducting materials are characterized by a specific heat at low temperatures that is two or three orders of magnitude higher than that of normal metals [1]. This results in a conduction-electron effective mass some hundred times the free-electron mass. The physical origin of the large mass and unusual superconducting and magnetic properties is the strong coupling between the conduction electrons and local f-electron moment fluctuations characteristic of these materials [1]. The following section will discuss the most important features of these novel materials.

1.1 Heavy Fermions

At room temperature and above, heavy electron systems behave as a weakly interacting collection of f-electron moments and conduction electrons with ordinary masses. As the temperature is lowered the f-electron moments become strongly coupled to the conduction electrons and to one another, and the conduction-electron effective mass is typically several orders of magnitude the bare electron mass. Some of these systems are 'normal' with no magnetic ordering, others antiferromagnetic and some are even superconducting [Table 1.1]. The latter being a surprising result given that in ordinary superconductors a dilute concentration of magnetic impurities destroys superconductivity [1]. Moreover, in these materials the physical mechanism responsible for superconductivity is believed to

	Ordering Temperature (K)
Antiferromagnetic	
$UAgCu_4$	18.15
URu_2Si_2	17.0
UCu_5	15.2
U_2Zn_{17}	9.7
UCd_{11}	5.0
Superconducting	
URu_2Si_2	1.5
UBe_{13}	0.9
$CeCu_2Si_2$	0.65
UPt_3	0.50
No Ordering	
$UAuPt_4$	0.15^1
$CeAl_3$	0.02^1
$CeCu_6$	0.02^1
UAl_2	0.02^1

Table 1.1: Ordering in some heavy fermion systems. [1]Lowest temperature at which measurements have been made [1].

be an attractive interaction between electrons that results from an exchange of local moment fluctuations, rather than the exchange of phonons that leads to superconductivity in ordinary metals [1].

Some unique features of the low temperature normal state properties of heavy electron systems are:

1) A very large specific heat. As the temperature goes to zero, we can write the specific heat $C(T)$ in the form:

$$\frac{C(T)}{T} = \gamma + BT^2 \tag{1.1}$$

where γ is the electronic specific heat and B characterizes the contribution of the phonons to the specific heat. In heavy fermion systems γ is so large that the BT^2 terms

can be ignored (at least up to approximately 20 K). Since the electronic specific heat is not linear in temperature, one often writes $C(T)/T = \gamma(T)$.

In contrast to conventional metals, the magnetic susceptibility χ for heavy fermion systems exhibits considerable temperature dependence at low temperatures (below 20 K).

The specific heat coefficient, γ, shows a variety of dependences, the most prominent of which is a rapid decrease with temperature. Only at very low temperatures does χ become relatively constant with a value, like γ, that is quite enhanced over that of conventional metals. In Table 1.2, extrapolated zero-temperature values, $\gamma(0)$ are listed. The most important fact concerning γ is its large enhancement relative to that of conventional metals [Figure 1.1].

Type of Material	Specific Heat Coefficient $\gamma(0)$ $mJ/mole - K^2$
HF Superconductor	450 (UPt_3)
HF Magnet	400 (U_2Zn_{17})
Normal HF	1600 ($CeAl_3$)
Conventional Metal	9.4 (Pd)
Conventional Metal	0.6 (Ag)

Table 1.2: Extrapolated zero-temperature values of the specific heat coefficient γ . HF = Heavy Fermion. [2].

2) A transport property that characterizes metals is a low resistivity. The heavy fermion systems have room temperature values that are enhanced over conventional metals but not by so much that the systems are not still metals. Typical values of the resistivity are compared with conventional metals in Table 1.3.

As the temperature decreases from room temperature the resistivity of a heavy

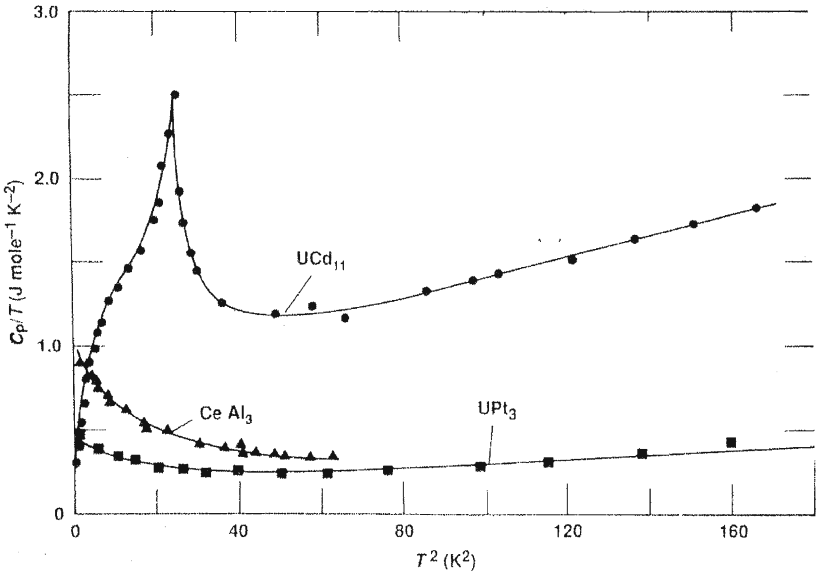

Figure 1.1: Specific heat at constant pressure for some heavy fermion systems [1].

fermion metal typically increases while that for a conventional metal decreases. Nonetheless at a sufficiently low temperature the resistivity of the heavy fermion system turns downward and for very low temperature in many cases has a T^2 dependence, i.e., $\rho(T) = \rho(0) + AT^2$. The last column of Table 1.3 shows the enormous enhancement of the A coefficient over conventional metals. The temperature dependence of the resistivity of several heavy fermion compounds is given in Figure 1.2.

1.2 UBe_{13} - Previous Studies

The low-temperature thermal- and transport-properties of ordinary metals are usually governed by their conduction-electron structure, resulting in characteristic temperature dependences of physical quantities like the specific heat or the electrical resistivity. Qualitative differences are observed in metallic materials where the electronic subsystem is

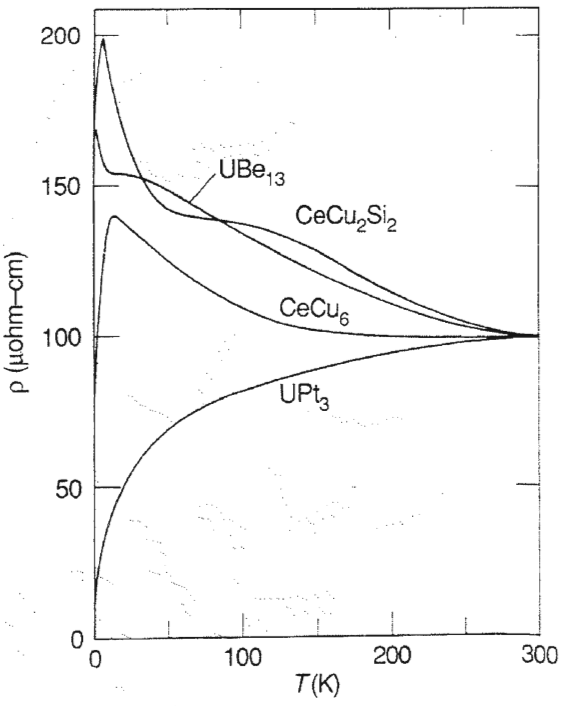

Figure 1.2: Resistivity of several heavy fermion systems [1]. Note that the resistivities at room temperature have been normalized to the same values.

governed by localized electrons like in d-, or even more pronounced, in f-electron materials. Such differences are found in the heavy fermion superconductor UBe_{13}.

UBe_{13} crystallizes in a cubic $NaZn_{13}$ structure with a remarkably large nearest neighbour U-U distance of 5.13 Å[3]. Figure 1.3 shows 8 unit cells of the structure of UBe_{13}. In this Figure one can observe the Uranium atoms sitting in the corners of the unit cell, while the Beryllium atoms are located in the interior.

Since the discovery of superconductivity in UBe_{13}, the vast majority of published data have been achieved on good-quality samples with a superconducting transition temperature, T_c, around 0.9 K. However, low-temperature specific-heat and thermal-expansion measurements on high-quality single crystals of UBe_{13} combined with literature results

Type of Material	Room Temperature Resistivity $\rho(RT)$ $\mu\Omega cm$	T^2-Coefficient of Resistivity A $(\mu\Omega cm)/K^2$
HF Superconductor	150 (UPt_3)	3 (UPt_3)
HF Magnet	110 (U_2Zn_{17})	not meaningful
Normal HF	170 $(CeAl_3)$	35 $(CeAl_3)$
Conventional Metal	20 (Pd)	10^{-5} (Pd)
Conventional Metal	2 (Ag)	10^{-7} (Ag)

Table 1.3: Typical values of the room temperature resistivity of heavy fermions (HF = Heavy Fermion).

give evidence for the existence of two variants of this compound. They have been classified by Langahammer and collaborators according to their superconducting transition temperatures into H-type (high T_c :$0.85 \leq T_c \leq 0.95$K) and L-type (low T_c:$T_c \approx 0.75$ K). Since L-type characteristics are only found for single crystals the determining factor leading to L- or H-type behaviour is most likely related to the details of the preparation process [4]. The research reported in this thesis was carried out using a single crystal of H-type. This single crystal was obtained from J. L. Smith at Los Alamos National Laboratory.

In Figure 1.4 typical literature curves for the ac-susceptibility, $\chi_{ac}(T)$, and the specific heat, $C_p(T)/T$ of UBe_{13} are shown. It may be seen that in both measurements the transition occurs around $T_c \approx 0.9$ K. The strong diamagnetic signal of $\chi_{ac}(T)$ alone gives no definite evidence for bulk superconductivity; however, the additional observation of a specific heat anomaly is convincing evidence for it [5].

The magnitude of the specific heat discontinuity at T_c is in fact proof that the large specific heat at T_c in the normal state is electronic in nature. This discontinuity has been reported to be even larger than that expected from BCS (Bardeen-Cooper-Shiffer) theory [Figure 1.5], pointing to strong coupling effects [3].

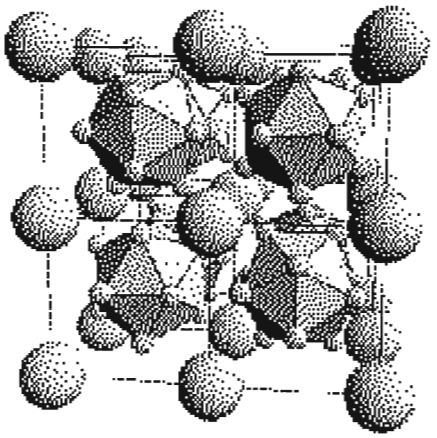

Figure 1.3: Crystal Structure of UBe_{13}.

The temperature dependence of the electrical resistivity, $\rho(T)$, of UBe_{13} has been described as one of the most striking of the heavy fermion systems. Shown in Figure 1.6, the resistivity at high temperatures has a negative slope. As temperature is lowered a 'shoulder' near $T_{M2} \approx 10$ K is followed by a maximum near $T_{M1} \approx 2.5$ K. Below T_{M1} the 'gradual' decrease in $\rho(T)$ is interrupted by the transition to superconductivity near $T_c \approx 0.9$ K [6]. The similarity in the shape of $\rho(T)$ for UBe_{13} to that of $CeCu_2Si_2$ [Figure 1.2] has led to a similar interpretation of the two maxima in the resistivity. The maximum at T_{M1} being due to the the onset of coherent scattering which develops at low temperatures. The higher temperature maximum at T_{M2}, again in analogy to $CeCu_2Si_2$, has been explained as scattering by crystal field levels [6].

The optical reflectivity, $R(\omega)$, of a UBe_{13} single crystal was measured over a broad spectral range extending from the far-infrared up to the ultraviolet by Bommeli *et. al.* [7]. The optical conductivity was obtained from Kramers-Kronig transformations applied to the measured optical reflectivity. Figure 1.7 displays the optical absorptivity $A(\omega) = 1 - R(\omega)$ reported. The most striking feature is the increasing $A(\omega)$ in the far-infrared

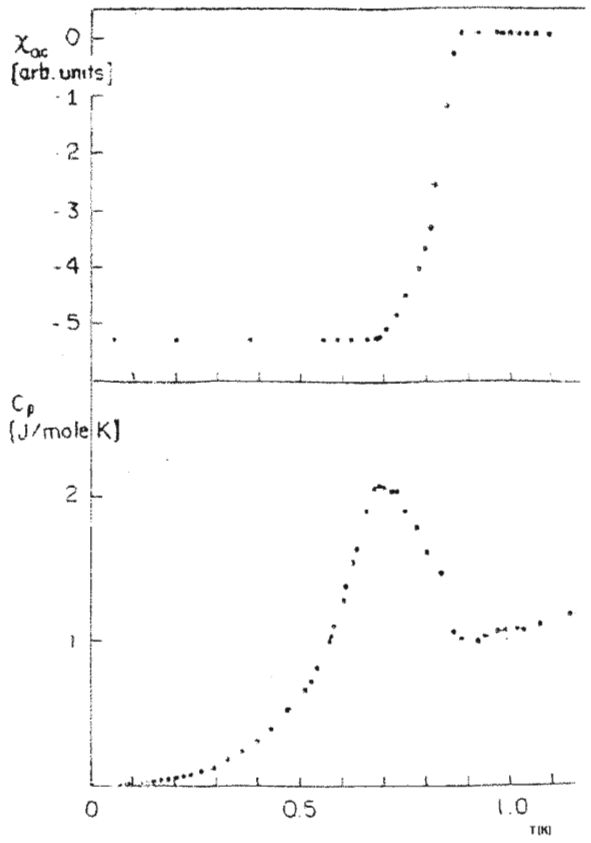

Figure 1.4: Specific heat and Magnetic susceptibility of UBe_{13} [5].

with decreasing temperature, which leads to a suppression of the far-infrared spectral weight (area under the curve of the optical conductivity) in $\sigma_1(\omega)$ [Figure 1.8]. It was also reported that measurements between 6 and 1.8 K did not show any further temperature dependence.

Far infrared reflectance measurements have also been reported by Bonn *et. al* [8] down to a temperature of 2 K. Shown in Figure 1.9 is the reflectance at four different temperatures [8]. Overall, the reflectance decreases as the temperature is lowered, which is in agreement with the work of Bommeli *et. al*.. This is in qualitative agreement with

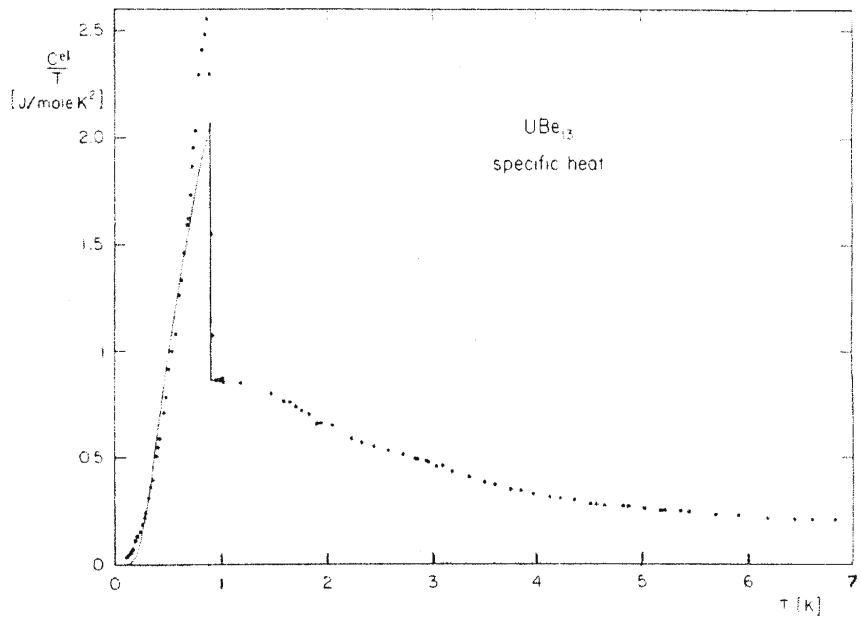

Figure 1.5: Specific heat of UBe_{13}. The solid line is the BCS prediction [3].

the observed increase in dc-resistivity as the sample is cooled. Figure 1.10 shows the real part of the optical conductivity reported by Bonn. At all temperatures measured the far-infrared conductivity rises with increasing frequency and the rise becomes steeper at 2 K. Since Drude theory predicts a conductivity which monotonically decreases with increasing frequency, the optical properties of UBe_{13} can not be attributed to free carriers with a frequency independent scattering rate.

This thesis presents a detailed study of the low temperature far-infrared optical properties of UBe_{13}, down to frequencies as low as 10 cm^{-1}. For the first time, the measurements extend into the superconducting state.

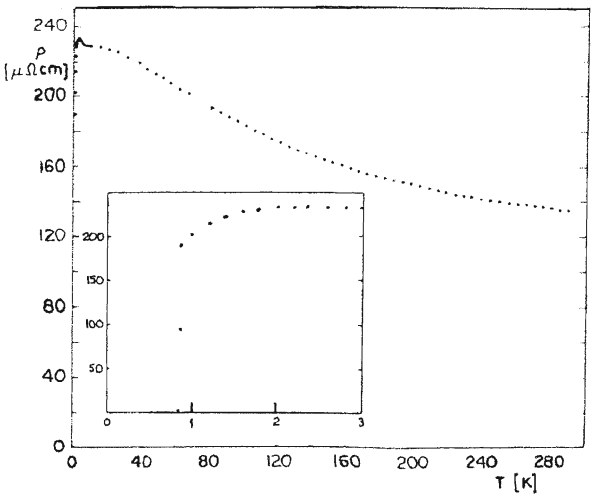

Figure 1.6: Resistivity of UBe_{13} [5].

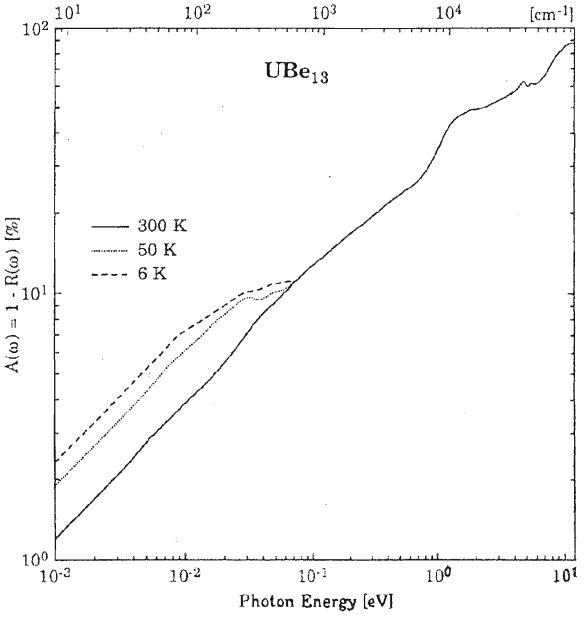

Figure 1.7: Absorptivity by Bommeli *et. al.* [7].

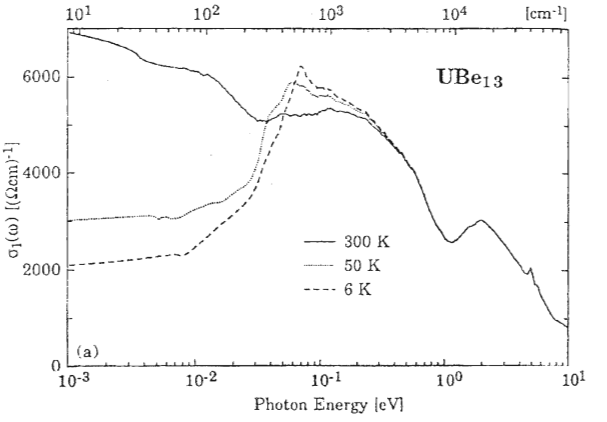

Figure 1.8: Optical Conductivity by Bommeli *et. al.* [7].

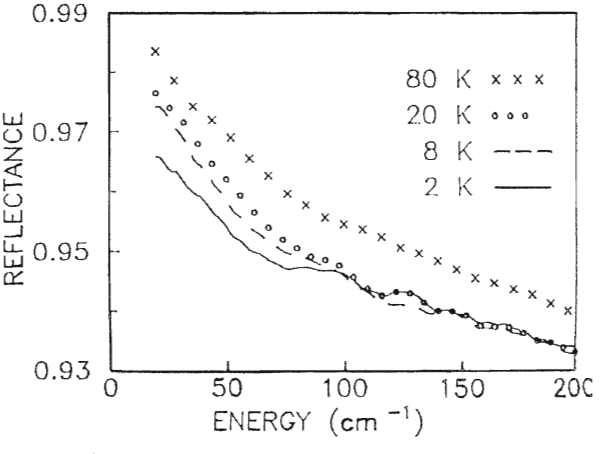

Figure 1.9: Reflectance measured by Bonn *et. al.* [8].

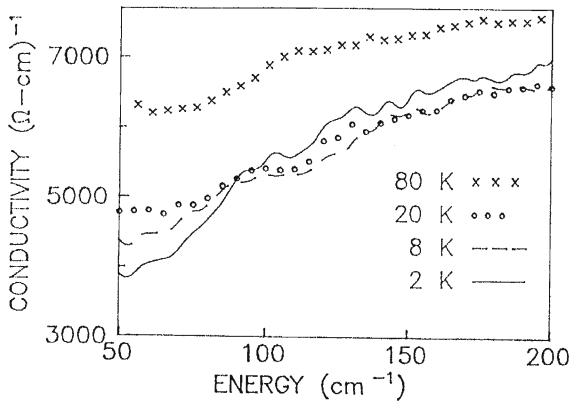

Figure 1.10: Optical conductivity determined by Bonn *et. al.* [8].

Chapter 2

Characterization of UBe_{13}

Many studies have been made on the heavy fermion material UBe_{13} during the past few years and many papers have been published. In these studies, two significantly different types of single crystals have been used, namely 'H'- and 'L'-type. Therefore, it was important to identify the type of sample used during the course of this research. DC-resistivity and AC-susceptibility are two popular characterization tools which provide this information.

An AC-susceptometer was configured for temperature dependent measurements within a He^3 cryostat while resistivity measurements were performed using an existing setup. These measurements covered a temperature range of 295 K, from 0.4 K to room temperature. The superconducting transitions of our particular samples were found at approximately 0.9 K which would categorize them as 'H'-type.

2.1 DC-Resistivity

2.1.1 Background

The temperature dependence of a sample's resistivity is an important tool for the characterization of a sample. Resistivity, ρ, is defined as:

$$\rho = R \times \frac{A}{L} \tag{2.1}$$

where R is the resistance, A the cross-sectional area of current flow, and L the length

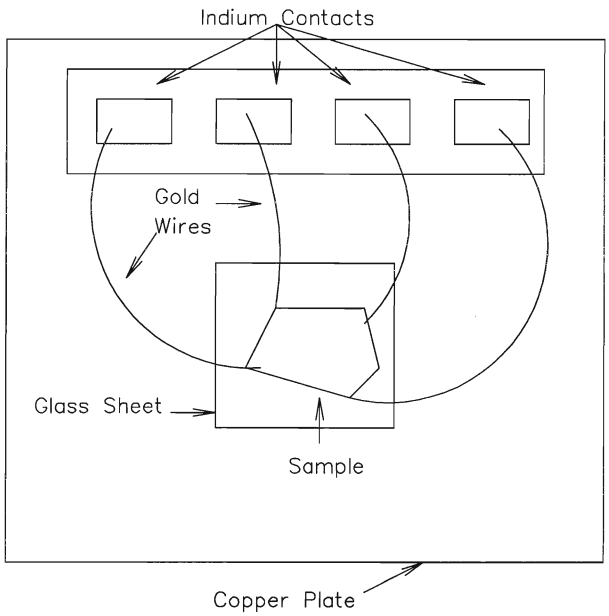

Figure 2.1: Typical sample configuration for resistivity measurements.

of the sample. Obtaining the cross-sectional area, A, of a sample can be a challenging task to accomplish in practice. Geometrical factors can be avoided by using a technique that allows resistivity measurements on arbitrarily shaped samples developed by van der Pauw [9] . This technique requires that the sample be of uniform thickness, that the surface of the sample be singly connected, and that the electrical wiring contacts are small and placed around the perimeter of the sample[10]. A detailed explanation of the van der Pauw technique is described in reference [9].

2.1.2 Experimental Details

Figure 2.1 shows the typical configuration of the contacts made on a sample mounted on a holder for a resistivity measurement. The sample is placed on a very thin glass sheet that is glued with five minute epoxy to a copper plate. This isolates the sample from the copper plate. Four gold wires are then attached to points along the perimeter

of the sample using silver paint. These wires are subsequently connected by pressing them firmly into four isolated Indium contacts. Silver paint is then added on top of the gold wires (on the Indium contacts) to avoid disconnections during the resistivity measurements.

The sample is then placed on the bolometer stage of the He^3 cryostat, and the wires from the Indium pads are connected to the appropriate pins inside. The cryostat is then cooled to 0.4 K and slowly warmed up to room temperature. The data collection procedure for the DC-Resistivity is described in detail in reference [10].

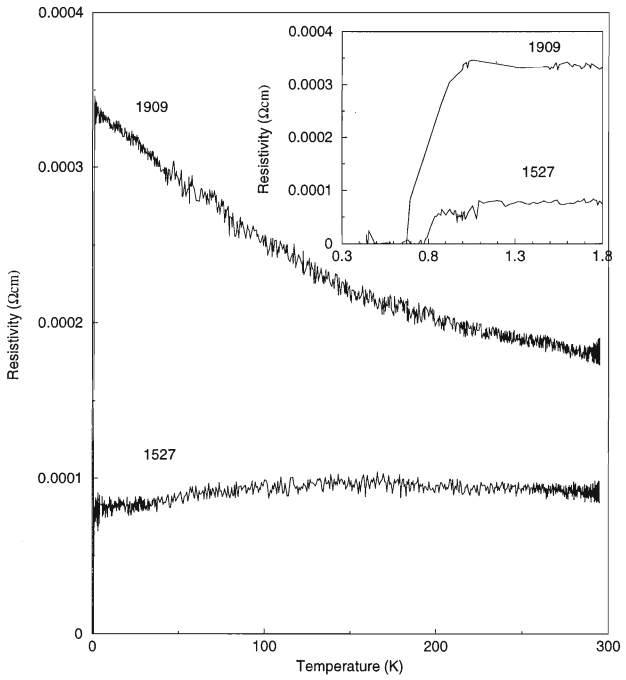

Figure 2.2: Resistivity of UBe_{13}. Inset shows the transitions.

2.1.3 Results

Three very important resistivity measurement were performed on two different UBe_{13} samples. The first and second measurements were done on samples 1909 and 1527 (batch

numbers provided by Los Alamos National Laboratories) following the procedure described in section 2.1.2. These are shown in Figure 2.2. Notice the difference in the overall resistivity of the two samples. Sample 1909 showed a consistently higher resistivity as compared with its counterpart 1527.

The results for sample 1909 are in good agreement with other measurements published in the literature. It shows a rise in the resistivity as the temperature is lowered. This rise results in a peak, which is observed at approximately 1.5 K. The sudden drop at 1.5 K is attributed to a coherent state interrupted by a superconducting state, which occur near the same temperature. Upon closer inspection one can observe that this transition occurs at the expected value of $T_c \approx 0.9\ K$ for samples of 'H'-type.

Our other sample, namely 1527, has a different shape in its resistivity. Although one can not be one hundred percent certain, this deviation from the expected result might be attributed to impurities or other imperfections that occurred while it was prepared. This was an important point for our experimental experience, since it was decided to use sample 1909 for subsequent reflectance experiments. In general, one can assume that large changes in a sample's resistivity translate to greater differences in the temperature dependence of its' absolute reflectance.

The third resistivity measurement was performed on the 'sample stage' of the He^3 cryostat. Reflectivity experiments are performed using this stage and the temperatures used to report our data are very important. The sensor used to determine the temperature in the sample stage is located several centimeters away from the location of the sample itself. Therefore, it is conceivable that the temperature reading of this sensor does not match the actual temperature at which the sample is. This final resistivity measurement was done for the purpose of determining whether or not the sample goes through the superconducting transition while placed at this location. Figure 2.3 shows the configuration used for this experiment. Note that the sample is mounted with the

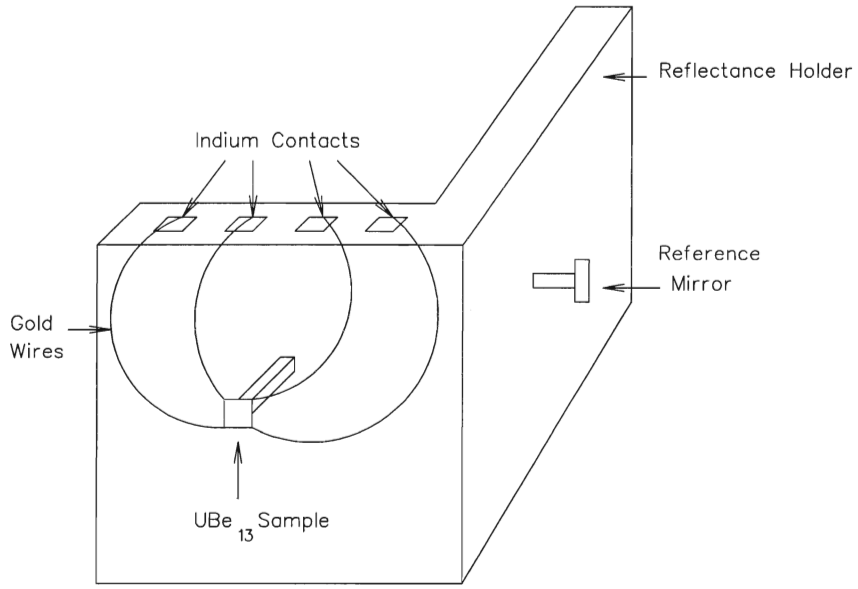

Figure 2.3: Resistivity setup on the sample stage of the cryostat.

same configuration as one would use for a reflectance experiment. In fact, the resistivity measurement was carried out immediately after a reflectance measurement without remounting the sample.

The result is shown in Figure 2.4. This figure shows that the transition was also obtained by placing the sample at this location, however it appears broader and zero resistance is not obtained down to 0.5 K. This suggests that the cryostat is on the verge of reaching temperatures below the superconducting transition of the sample when it reads 0.5 K. During a reflectance experiment the temperature of the sample could be slightly lower since it was observed that the current used for the resistivity experiment produced a load on the He

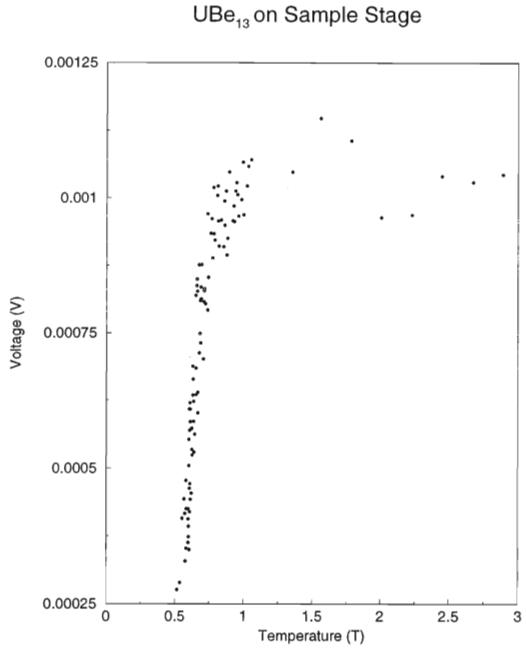

Figure 2.4: Resistivity of UBe_{13} mounted on the sample stage.

2.2 AC-Susceptibility

2.2.1 Background

Field and temperature dependence of the AC-Susceptibility of a sample has become an established tool for investigating magnetic and superconducting materials [11]. The susceptibility of a sample is defined as:

$$\chi = \frac{\partial M}{\partial H} \tag{2.2}$$

where M is the magnetization and H the applied magnetic field [12]. This technique offers a non-invasive confirmation of magnetic and superconducting transitions that may occur in a sample.

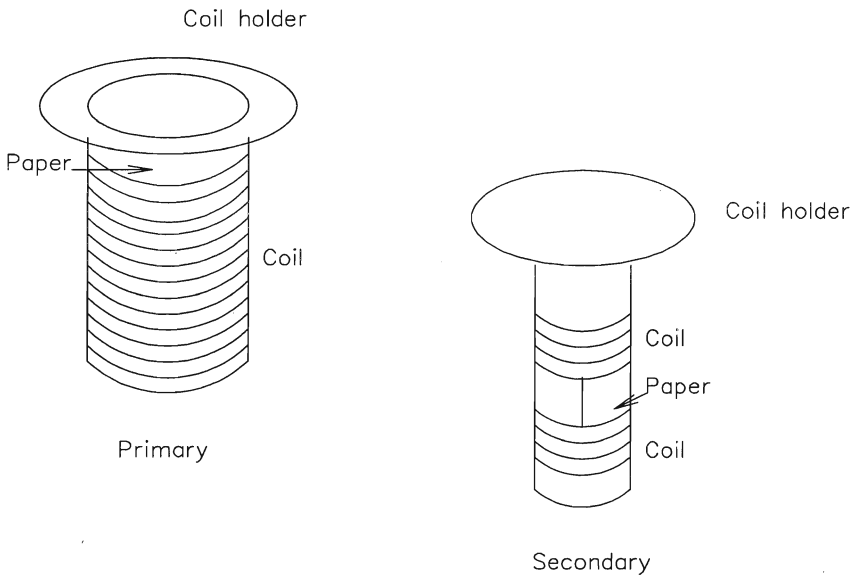

Figure 2.5: Diagram of the primary and secondary coils of the AC-susceptometer

2.2.2 Experimental Details

AC-susceptibility measures a change in the mutual inductance of a primary and two identical but oppositely wound secondary coils when a sample is placed in one of the secondary coils. Both of these coils were wound with a computer controlled lathe using Alcatel Scanwire (Taurimide 200 NAT, AWG 40 H [40 HAMT]) [13] .

As shown in Figure 2.5, the primary coil consisted of ten equal layers and had nearly 7000 turns in total, with a length of 6 cm and an inside diameter of 4 cm. Each secondary coil consisted of 20 layers, with a length of 1.5 cm and an inside diameter of 2.5 cm. These coils were then coated with GE varnish to ensure complete isolation from one another.

The two secondary coils are connected in series so that the output is nearly balanced without the presence of a sample. Any small off-balance signal is balanced electronically [14] . The circuit diagram is shown in Figure 2.6.

The sample is then placed on a holder, shown in Figure 2.7, and mounted on the

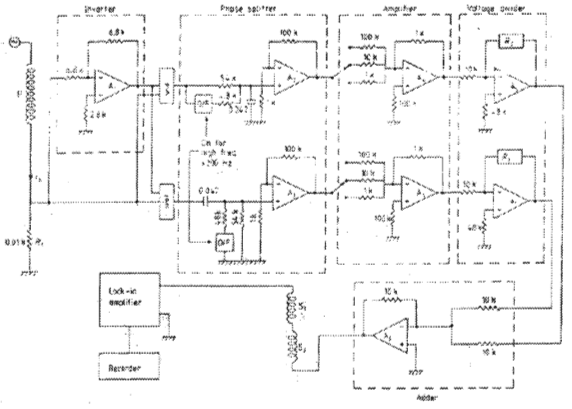

Figure 2.6: Circuit diagram for electronic balancing of secondary coils [14].

bolometer stage of the He^3 cryostat. The temperature is lowered to 0.4 K as described in section 3.2.1. The sample is then left at this temperature for a few hours, in order to allow the temperature to equilibrate within the He^3 stage and sample holder. The temperature is then allowed to begin to rise by disconnecting the bolometer He^3 stage charcoal pump switch a total of 3 to 4 turns. This provides a temperature rise of approximately 1.2 K, to 1.6 K, over a period of 4 hours. The He^4 stage is gradually and continuously brought in contact with the He^3 stage using another heat switch to allow a further rise in temperature to 4.2 K. This may occur quite rapidly. If one wishes to have a more controlled rise for this range, one must pump on the He^4 bath to bring it down to approximately 1.85 K, at this point one would connect the bolometer heat switch for the He^4 stage, and gradually release the vacuum on the He^4 bath.

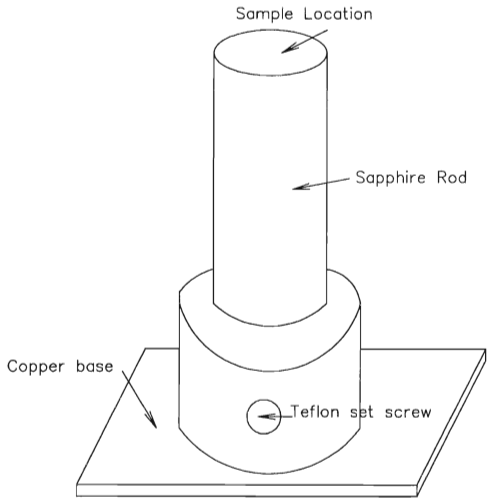

Figure 2.7: Sample holder for the AC-susceptometer.

2.2.3 Results

Temperature dependent measurements of the AC-Susceptibility of UBe_{13} sample 1909 were carried out. Figure 2.8 shows a discontinuity at around T_c, 0.9 K. This is again evidence that a magnetic transition, namely the diamagnetic transition of a superconductor, has taken place.

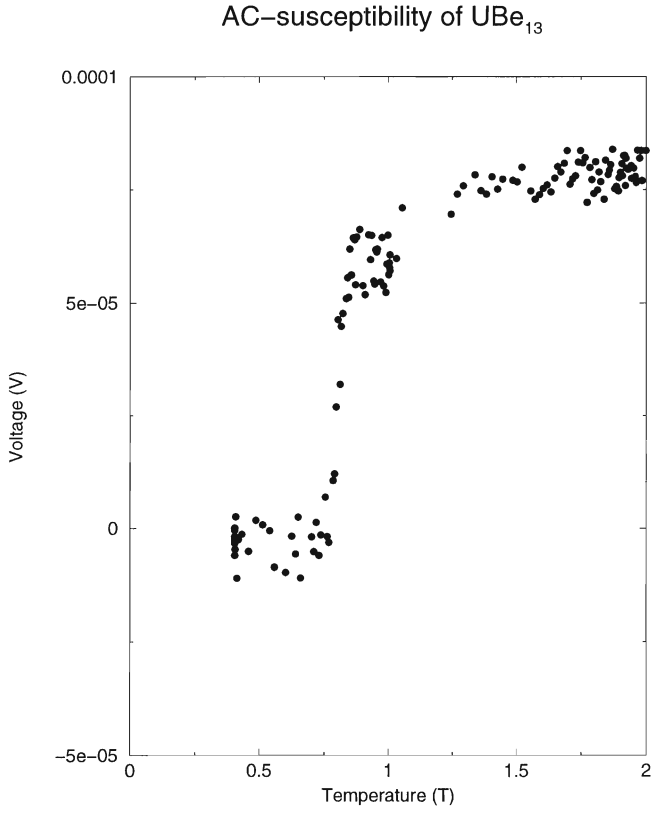

Figure 2.8: Susceptibility of UBe_{13} sample 1909.

Chapter 3

Normal and Superconducting State Optical Properties of UBe_{13}

In this chapter the optical properties of the UBe_{13} single crystal sample 1909 will be discussed. A literature review of relevant experimental data concerning UBe_{13} has been presented in Chapter 1. To date, none of these studies have shown the optical properties of this sample below the superconducting transition temperature of 0.9 K. In this thesis, seven different temperatures, namely 0.5, 0.75, 1, 10, 45, 85, and 300 K, have been explored. This provides the first, to the best of our knowledge, optical investigation of this sample in the superconducting state.

3.1 Background

Measurements of the temperature dependent reflectance usually involve three main experimental components: an interferometer, a cryostat, and a detector. The raw output obtained is called an interferogram, which is a plot of the output voltage of the detector versus the position of the movable mirror in the interferometer. A Fourier transform is usually performed on this interferogram, resulting in a power spectrum, which is a plot of intensity versus frequency. The power spectrum of the sample is then compared with the power spectrum of an intermediate reference by dividing the former with the later. The procedure is repeated after an in-situ gold evaporation of the sample. The final absolute reflectance, $R(\omega)$, is obtained using the following formula:

$$R(\omega) = \frac{\frac{UnCoated\ Sample}{Intermediate\ Reference}}{\frac{Gold\ Coated\ Sample}{Intermediate\ Reference}} \tag{3.1}$$

The intermediate reference is used to avoid errors caused by small variations in the operating temperature of the detector, and other ambiant changes that may occur during the collection of data. The gold coated sample is also used as a reference. The use of gold introduces an error in the measurement which is negligible. This is to eliminate any inconsistencies derived from geometrical considerations of the actual sample (roughness of the sample surface, etc.), and any change in position of the sample that may occur because of expansion of the metal components inside the cryostat, while changing from the very low to much higher temperatures.

3.2 Experimental Details

The experiments performed on the single crystal of UBe_{13} were carried out using two different experimental setups, one being at Brock University and the other at McMaster University. The former covered a range of 110 cm^{-1} from 10 to 120 cm^{-1}, and a temperature range between 0.5 and 85 K. The latter covered a range of 750 cm^{-1}, from 50 to 800 cm^{-1} and temperatures ranging between 20 K and room temperature. For the purpose of calculations, data obtained from 400 to 32,000 cm^{-1} was also collected by Graeme Wardlaw, details of these experiments are fully explained in reference [15]. A brief description of the main components of the two experimental setups and procedures follows.

3.2.1 The Martin Puplett type Polarizing Interferometer and the He^3 Cryostat - Brock University

The Martin Puplett polarizing interferometer provides a plot of the reflected intensity versus frequency via a Fourier transform. It contains a mercury-xenon light source which is directed via mirrors through a polarizing grid and a polarizing beam splitter. The light is split and travels along two paths, one to a fixed mirror and the other to a movable mirror. It is then recombined at the beam splitter after reflecting from the mirrors and the resulting interference pattern is then directed out of the spectrometer through a polarizing chopper towards a Helium 3 cryostat, and to the sample or intermediate reference via one of two wave guides.

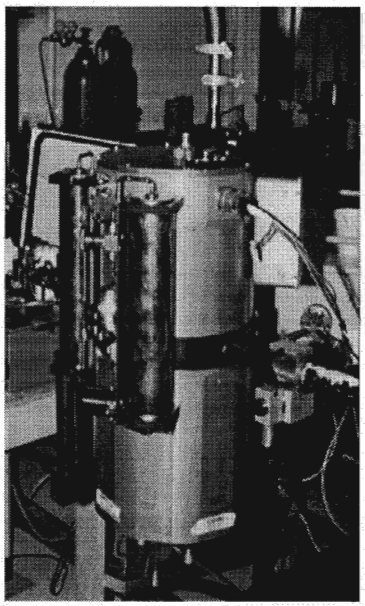

Figure 3.1: Picture of the Brock University Cryostat.

The cryostat is shown in Figure 3.1. This cryostat is used to cool in two stages the sample to temperatures of approximately 0.5 K. In the first stage, He^4 is used

to cool most of the internal components. This is done by transfering liquid He from a storage dewar into the cryostat. The He^4 cavity is then pumped for about 2 hours after which the pump is turned off. This reduces the temperature to approximately 2 K (which is a temperature below the condensation point of He^3). The second stage involves the condensation of internally stored He^3 gas which is recycled every experiment. The temperature of the He^3 liquid is lowered to 0.5 K by using a charcoal absorption pump to reduce the vapor pressure above the liquid He^3. Once reaching this temperature, the sample is left to equilibriate for approximately two hours. A subtle but important point is that before starting any collection of data, one must bring the He^4 bath in the cryostat to atmospheric pressure. Normally this bath would eventually reach this pressure by the slow evaporation of the He^4 liquid once the pump is turned off. This proved to be causing problems in the consistency of the data collected. Small drifts of the intermediate reflectance (approximately a 2 % increase over a period of 3 hours) were observed when the dewar was not brought up to atmospheric pressure.

The detection was accomplished using a bolometric sensor. This sensor measures the temperature change when a photon hits its surface. Therefore, a constant temperature for this sensor must be maintained. The measurements were carried out using a bolometer which worked at 0.4 K. These sensors use electronic methods to avoid any drifts in the signal. One of these methods is to apply a bias voltage. Different filtering configurations and different bolometers use different bias voltages. The best method to determine this voltage is to obtain a 'load curve'. A load curve is a graph of the bolometer's voltage versus the bolometer's current for different bias voltages. A sample of a load curved is shown in Figure 3.2. Notice that at first the current rises slowly and then it dramatically shoots upwards as the bias voltage is increased. By using the manual provided by the manufacturer of the cryostat [16], one obtains the optimal bias voltage through the intersection of a tangent at the inflection point with the x-axis (voltage axis).

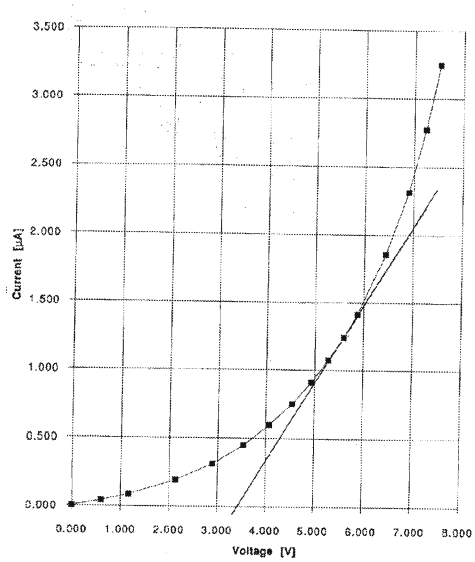

Figure 3.2: Sample load curve for bias voltage determination [16].

The temperature of the sample was measured via two temperature sensors mounted on the sample stage. These sensors were only used to measure the temperature between scans and were turned off otherwise with the cable disconnected. This was done to avoid noise introduced by electrical connections near the sample.

At each temperature the sample and reference are measured about 36 times each and averaged out to obtain the final result. This is repeated for the gold coated sample.

3.2.2 Fast Fourier Transform Interferometer - McMaster University.

As we will see in section 3.3.1, one must obtain all frequencies to perform a Kramers-Kronig analysis. Due to the limited frequency range of the spectrometer at Brock, another experiment was performed at McMaster University. The experimental setup consisted of a Michelson interferometer, a He^4 cryostat and a bolometric sensor, similar to the one used at Brock, which was contained within another He^4 cryostat.

The Michelson interferometer, as the name suggests, consisted of a fixed and a movable mirror. The latter moved at a very fast rate on an oil lubricated bearing. To ensure smooth operation the oil pool was pumped and recycled every thirty minutes. The position of this movable mirror was monitored via the interference pattern of a laser beam and its zero path via a separate white light interferogram.

The sample was placed within the small He^4 cryostat that was capable of obtaining temperatures as low as 14 K. The temperature was monitored constantly via a sensor mounted near the sample. The bolometric detector was contained within another He^4 cryostat and had an operating temperature of 4.2 K.

The collection of data was accomplished using an in-house program, which performed a fast Fourier transform after every cycle of the movable mirror. An average of fifty cycles was performed to obtain the final power spectrum. An identical measurement was carried out on the reference mirror, and ratios of sample to reference were calculated to obtain the intermediate reflectance. This was repeated for about 18 times and averaged for the final reflectance result at each temperature. After all temperatures were collected, a thin layer of gold was evaporated in-situ on the sample and the same procedure was repeated. The final reflectance was calculated using equation 3.1.

3.3 Reflectance of UBe_{13} - Experimental Results

In Figure 3.3 the reflectance of UBe_{13} for seven different temperatures is shown. The low frequency cutoff of the 300 and 85 K data, the former collected at McMaster and the latter at Brock, is higher than other temperatures, due to limitations of the experimental setups. The remaining temperatures are shown from 10 to 110 cm^{-1}. It is worth mentioning that higher frequency measurements have also been made for most of these temperatures but have not been shown since they fall outside of the frequency range of interest for this

thesis.

Overall the reflectance increases with decreasing frequency. Also, one can see that the reflectance decreases as the the temperature is lowered. This is obvious between the temperatures of 300 to 10 K, and not so obvious between 10 and 0.75 K. This is in qualitative agreement with the increase in the dc resistivity as the sample is cooled. These results are also in agreement with the previously published results by Bommeli [7]. The reflectance changes quite noticeably between 0.75 and 0.5 K. The 0.5 K reflectance is higher than that of 0.75 K at low frequencies, and lower at high frequencies with the cross over near 45 cm^{-1}. At 0.5 K the dc resistivity is zero because of the onset of coherence and the superconducting transition.

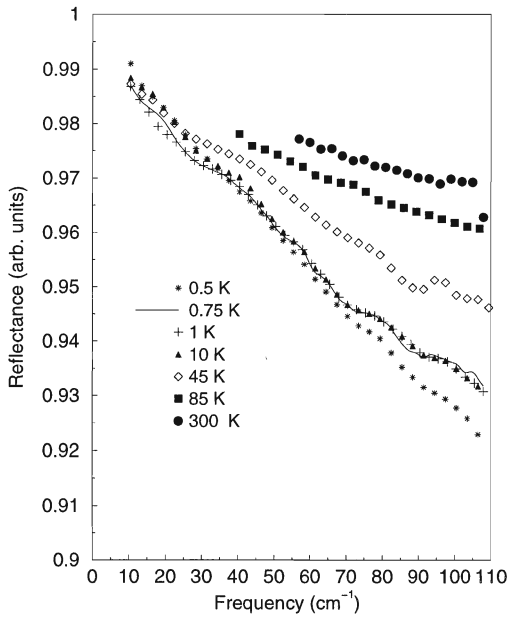

Figure 3.3: Reflectance of UBe_{13}.

3.3.1 Mathematical Analysis using Kramers-Kronig Relations

The optical conductivity of a sample is obtained from Kramers Kronig transformations applied to the reflectance data measured. These transformations are based on an integral that involves the reflectance of a sample throughout the entire frequency range (from zero to infinity). Our reflectance measurements covered a range from 10 to 105 wavenumbers approximately. Low frequency extrapolation had to be made by observing the general behaviour of the noisy data obtained in our experiments below 10 wavenumbers. In general, metallic samples would have a reflectance of unity at zero frequency; this has been assumed as true for our sample. Therefore, a straight line was used from the point of the reflectance at 10 wavenumbers, to unity at zero frequency. Measurements performed at McMaster University had a higher frequency limit of 700 cm^{-1}. Data between 700 and 32,000 cm^{-1} was provided by Graeme Wardlaw [15]. For the high frequency range, between 32,000 to 240,000 wavenumbers, digitized data from Eklund et. al. [17] has been used. For frequencies higher than 240,000 wavenumbers a power law, ω^{-4} decay was assumed, which is the expected free-electron behaviour. The Kramers Kronig relations are discussed further in Appendix A.

3.4 Optical Conductivity of UBe_{13} - Experimental Results

Figure 3.4 shows the real part of the optical conductivity of UBe_{13} for frequencies ranging from 10 to 210 wavenumbers. Overall, the optical conductivity decreases as the temperature is lowered. Again, this is obvious for temperatures between 300 and 10 K, and then down to 0.5 K. Between 10 and 0.75 K this decrease is not as obvious. The optical conductivity data also shows the development of a broad minimum for temperatures at 45 K and below.

Similar behaviour has been reported for another heavy fermion system, namely URu_2Si_2,

by Bonn et.al. [18]. URu_2Si_2 has a coherence temperature, T_{co}, of 70 K and an antiferromagnetic transition at 17.5 K. Measurements done at 90 K for this system showed a flat optical conductivity, similar to our measurements between 300 and 85 K. Furthermore, URu_2Si_2 shows a broad minimum for temperatures below 70 K, again similar to the minimum seen in UBe_{13} at 45 K and below.

The dc-conductivity values are marked on the conductivity axis of Figure 3.4 [19]. Note, that there is quite reasonable agreement between the trend of the optical conductivity at the lowest frequency measured and the dc values for 45 K and 10 K. At 85 K and 300 K the dc values are lower than the limit of the optical data. While this might be attributed to experimental error, the 85 K optical conductivity has a slight downward trend at the lowest frequencies suggesting that this might be a real effect.

The optical conductivity shown in Figure 3.4 is decidedly non-Drude like. The Drude conductivity which can be described by a frequency independent scattering rate is Lorenzian in shape, and centered at zero frequency. The Drude conductivity thus monotonically decreases with increasing frequency.

To analyze the behaviour of the optical conductivity of UBe_{13}, one can use an extension of the Drude Theory [20] which involves a frequency dependent scattering rate, $\Gamma(\omega)$, explained in the following section.

3.5 Frequency Dependent Scattering Rate of UBe_{13} - Experimental Results

The frequency dependent scattering rate is obtained from the optical conductivity using the following formula:

$$\Gamma(\omega) = \frac{\omega_p^2}{4\pi}\, Re\left[\frac{1}{\sigma(\omega,T)}\right] = \frac{\omega_p^2}{4\pi}\left[\frac{\sigma_1(\omega,T)}{\sigma_1^2(\omega,T)+\sigma_2^2(\omega,T)}\right] \tag{3.2}$$

where $\sigma_1(\omega,T)$ is the real part of the optical conductivity, $\sigma_2(\omega,T)$ is the imaginary

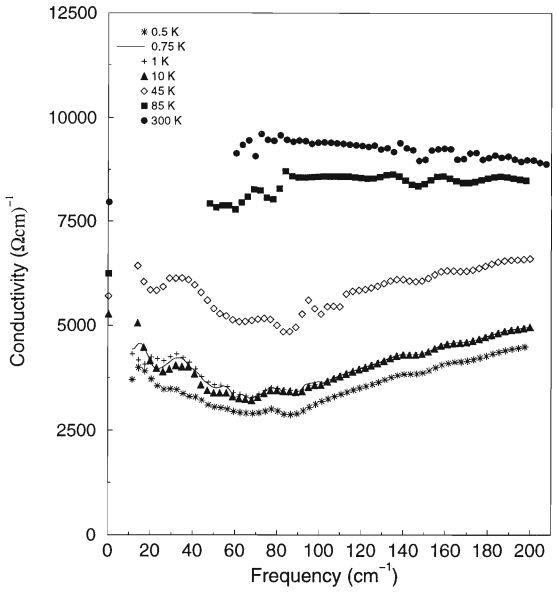

Figure 3.4: Real part of the Optical Conductivity of UBe_{13}. Y-axis shows dc-conductivity values taken from Knetsch et. al. [19].

part of the optical conductivity and ω_p the plasma frequency. Figure 3.5 shows the frequency dependent scattering rate between 10 and 210 cm^{-1}. At 300 K, and 85 K, $\Gamma(\omega)$ is nearly flat, somewhat decreasing as the frequency increases. But at 10 K and below, the scattering rate is suppressed at low frequencies and broadly peaks around 70 cm^{-1}. On this figure the calculated dc-values for the scattering rate were obtained through the following equation:

$$\Gamma_{dc} = \frac{\omega_p^2}{60\sigma_{dc}} \tag{3.3}$$

using resistivity values from Knetsch et. al. [19] and ω_p determined by Wardlaw [15]. The factor of 60 is equal to $4\pi(4.77)$ where 4.77 is a factor which converts units such that ω_p and Γ are given in cm^{-1} and σ_{dc} is in $\Omega^{-1}cm^{-1}$. Note that in equations 3.2 and 3.4,

that 4π should also be multiplied by this factor of 4.77 if these units are used.

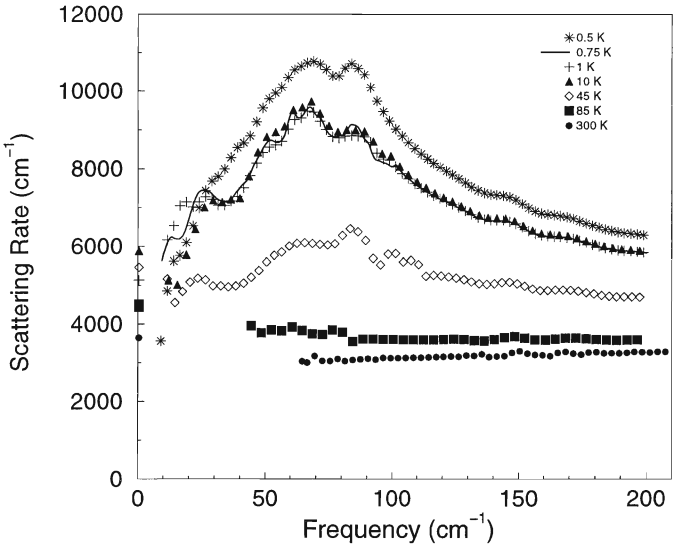

Figure 3.5: Frequency dependent Scattering Rate of UBe_{13}. Some calculated dc-values are shown along the y-axis [19].

To continue using the analogy of URu_2Si_2, similar behaviour was observed for $\Gamma(\omega)$. The emergence of this peak (at 110 cm^{-1} for URu_2Si_2) has been associated with the energy which separates the coherent behaviour from the regime of single impurity scattering. For UBe_{13}, our results would seem to indicate that the feature in the resistivity associated with this behaviour would be at a temperature which is no lower than 45 K.

3.6 Frequency Dependent Mass Enhancement of UBe_{13} - Experimental Results

The frequency dependent mass enhancement is obtained from the optical conductivity using the following formulas:

$$1 + \lambda(\omega) = \frac{1}{\omega}\frac{\omega_p^2}{4\pi}\, Im\left[\frac{1}{\sigma(\omega,T)}\right] = \frac{1}{\omega}\frac{\omega_p^2}{4\pi}\left[\frac{\sigma_2(\omega,T)}{\sigma_1^2(\omega,T)+\sigma_2^2(\omega,T)}\right] \tag{3.4}$$

Where $1 + \lambda(\omega) = m^*/m_e$ is the effective mass enhancement, ω is the frequency, $\sigma_1(\omega)$ is the real part of the optical conductivity, $\sigma_2(\omega)$ is the imaginary part of the optical conductivity, and ω_p is the plasma frequency, as explained before.

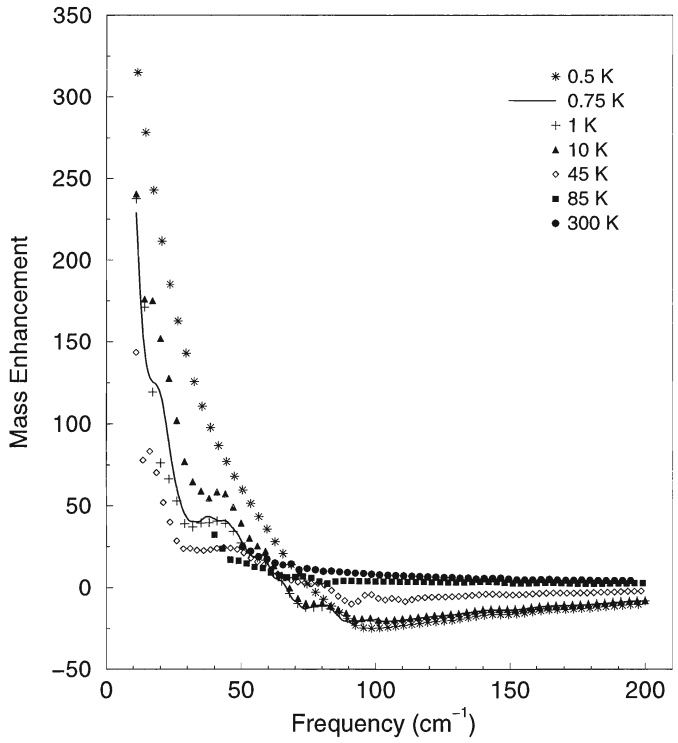

Figure 3.6: Frequency dependent mass enhancement of UBe_{13}.

Figure 3.6 shows the experimental results for the mass enhancement coefficient. At low temperatures, between 0.5 and 45 K, the mass enhancement is negative at high frequencies, crossing over to large positive values at low frequencies. At these temperatures a broad minimum is found around 80 cm^{-1}. This behaviour has also been observed in

URu_2Si_2. This behaviour is not observed at temperatures above 45 K. Also, as the temperature is lowered, its value as frequency approaches zero also increases. The low temperature values obtained for the mass enhancement coefficient are in good agreement with literature values [21].

3.7 Discussion

3.7.1 High Temperature Measurements

This chapter has presented the experimental results and shown the optical properties of UBe_{13} in the far infrared. The optical conductivity obtained is in partial agreement, namely the overall trend and level, with previously published data (see Chapter 1). Our work, however, indicates that the low frequency measurements (below 40 cm^{-1}) presented by Bommeli et. al. are not entirely reliable because they do not resolve the minimum in the conductivity.

For the work presented in this thesis, the low frequency cutoff was 10 cm^{-1} and one can observe a broad minimum in the optical conductivity for temperatures at 45 K and below. This behaviour of the optical conductivity, in which a minimum develops below a specific temperature, is similar to the behaviour of the optical conductivity of URu_2Si_2 [18], UPt_3 [22], and other heavy fermion systems [23] below the coherence temperature, T_{co}. This would suggest that coherent transport exists for UBe_{13} at temperatures as high as 45 K. A possible problem with this interpretation is that the resistivity continous to rise through this temperature. However, even after close to 20 years of study, the resistivity of UBe_{13} is still not well understood. The application of a magnetic field [6] or the addition of impurities [24] causes the resistivity to be suppressed at low temperatures for temperatures as high as 50 K (see Figure 3.8). This suppression has been explained by Schmiedeshoff et. al. [6] as a sharpening of crystal field levels from a depression

of the Kondo effect. The Kondo effect can be explained as the scattering of the free electrons of a metal from the local moment of a magnetic impurity. This scattering leads to a highly correlated manybody groundstate where the conduction electrons form a spin-polarized 'cloud' around the magnetic impurity. This cloud forms at temperatures below a characteristic 'Kondo Temperature', T_K, and leads to anomalous behaviour in the transport properties of dilute magnetic alloys.

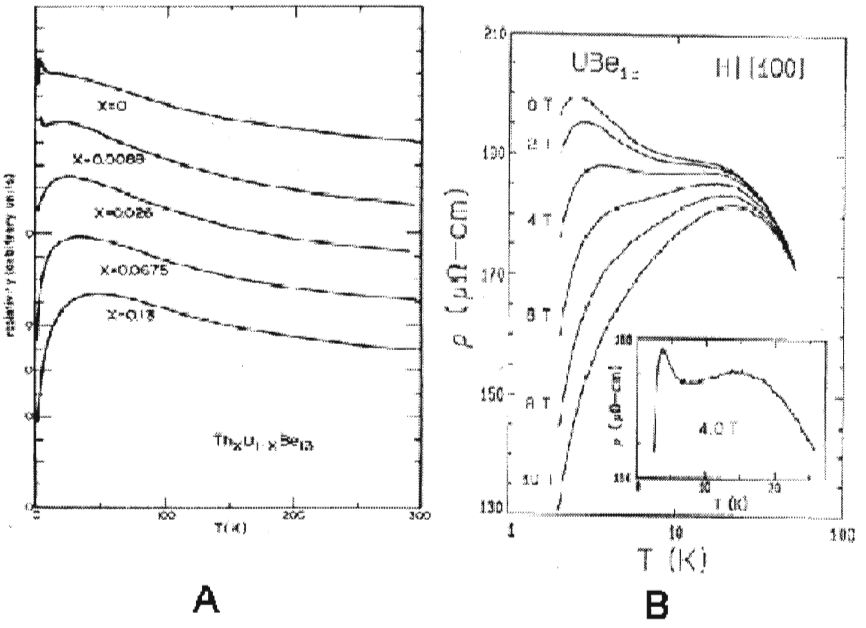

Figure 3.7: A. Resistivity of UBe_{13} with Thorium Impurities [24]. B. Resistivity of UBe_{13} with the application of a magnetic field[6].

Two interpretations for the appearance of such a minimum in the optical conductivity have been proposed. One, explained by Dordevic et. al., states that if the Kondo effect interaction dominates, theory predicts that hybridization between localized f-electron and conduction carrier states should lead to the opening of a charge gap (or pseudogap) at the Fermi energy [23]. Dordevic et. al. study two heavy fermion systems, which show

similar behaviour ($YbFe_4Sb_{12}$ and $CeRu_4Sb_{12}$). Both have a clear coherence temperature of $\approx 50K$, and show below the coherence temperature a narrow zero frequency centered resonance followed by a suppression of the optical conductivity at higher frequencies, which they associate with a gap like threshold.

A more thorough calculation which also takes into account the hybridization between f-electrons and conduction electrons has been presented by Mitrovic and Arberg[25]. In their work the behaviour of the optical conductivity of the Anderson impurity model has been determined in two different regimes: frequencies much greater than the coherence temperature, and frequencies much smaller than the coherence temperature. They found:

$$Re(\sigma(\omega)) = \frac{ne^2}{m^*}\frac{\tau^*}{1+(\omega\tau^*)^2} \; for \; \omega << T_K \tag{3.5}$$

$$Re(\sigma(\omega)) = \frac{ne^2}{m}\frac{\tau}{1+(\omega\tau)^2} \; for \; \omega >> T_K \tag{3.6}$$

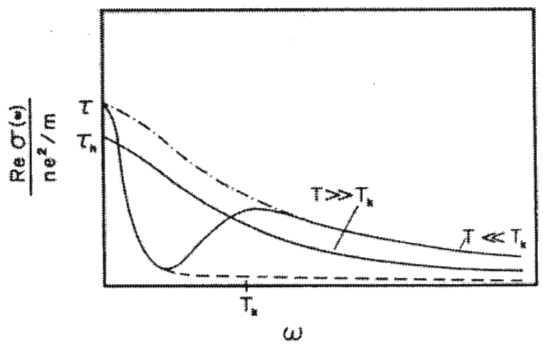

Figure 3.8: Temperature and Frequency dependent optical conductivity of the Anderson impurity model[25].

where $\tau = 1/\Gamma$ the relaxation time, and the rest of the symbols have their usual significance. A sketch of the frequency and temperature dependence of the optical conductivity is shown in Figure 3.9. Note that the exact shape of the cross-over region

was not calculated, however assuming a smooth cross-over, would yield a curve with a minimum near T_K as shown in this sketch.

3.7.2 Low Temperature Measurements

Measurements done in the superconducting state showed a further decrease of the optical conductivity as compared to the relatively temperature independent conductivity from 10 K to 0.75 K [Figure 3.4]. This is an interesting result since part of the rearrangement of the spectral weight that was lost could be the strong delta like peak expected at the origin due to the superconductivity. Figure 3.9 focusses on the scattering rate at 1 K and 0.5 K. In this figure one can observe a suppression of the scattering rate at low frequencies and an overall increase in absolute value at high frequency, for the superconducting relative to the normal state, with a cross over at $\approx 25\ cm^{-1}$. The dc value for the scattering rate has been calculated as described in section 3.5 and is shown in this figure for 1 K. Note that the low frequency value of the 1 K data seems to be in good agreement with the calculated value. The trend of the 0.5 K data is to approach a zero value for the scattering rate at zero frequency. This is the expected result for a zero frequency delta function in the optical conductivity in the superconducting state.

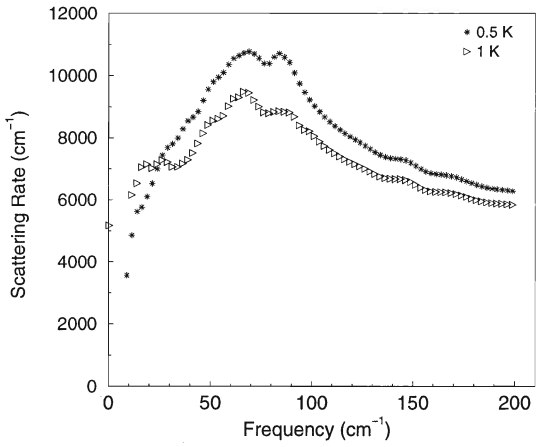

Figure 3.9: Frequency dependent Scattering Rate of UBe_{13} (low temperatures). The calculated dc-value at 1 K is shown on the y-axis.

Chapter 4

Conclusions

4.1 Remarks

The focus of this thesis has been the characterization and the study of the optical properties of UBe_{13}. The characterization results and the optical properties (reflectance and optical conductivity) at temperatures above 45 K are in general agreement with data published in the past. The important new results of this thesis are the emergence of a peak in the scattering rate for temperatures below 45 K, as well as the measurements at 0.5 K, which are in the superconducting state. The following sections summarize these findings.

4.2 Characterization Results

The resistivity of our sample of UBe_{13} increased as the temperature of the sample was lowered. This rise came to a maximum at approximately 2 K for our sample. This was followed by a sudden drop near 2 K which is attributed to a coherent state interrupted by a superconducting state. Upon close inspection it was found that the superconducting transition occurs at the expected value of $T_c \approx 0.9$ K. This is confirmation that our sample is of 'H'-type as explained in reference [7] . This was further confirmed with the observation of this transition in the AC-susceptibility, which was also found at 0.9 K.

4.3 Optical Properties

The absolute reflectance of UBe_{13} was obtained for seven different temperatures (300, 85, 45, 10, 1, 0.75 and 0.5 K). The reflectance was observed to increase with decreasing frequency. Furthermore, it was found that the absolute value of the reflectance decreased as the temperature was lowered. This was obvious between the temperatures of 300 and 10 K, but not so obvious between 10 and 0.75 K. This is in qualitative agreement with the increase in the dc resistivity as the sample is cooled. This trend is also in agreement with previously published results by Bonn and Bommeli [7]. In this thesis the reflectance has been measured for the first time at 0.5 K which is below the onset of coherence and well into the superconducting state. A significant change was observed between 0.75 and 0.5 K. The reflectance decreased more rapidly with increasing frequency at high frequencies. A cross-over to higher reflectance at low frequencies occurred near $\approx 45cm^{-1}$.

The real part of the optical conductivity of UBe_{13} was obtained for frequencies ranging from 10 to 210 cm^{-1} using Kramers Kronig transformations. Overall, the optical conductivity decreases as the temperature is lowered. These results are again in agreement with previously published data. This decrease in the optical conductivity translates into a loss of spectral weight in this region of the spectrum as the temperature is lowered. The development of a broad minimum occurring for temperatures at and below 45 K was also observed. This minimum was not reported by Bommeli et. al. and occurs near the lower limit of the data presented by Bonn et. al.

The frequency dependent scattering rate was obtained by applying equation 3.2 to the experimental results of the optical conductivity. For temperatures above 85 K a relatively flat, yet slowly decreasing scattering rate was found. The development of a peak occurred for temperatures below 45 K. In comparison with results published for

URu_2Si_2 this peak has been explained as the characteristic energy associated with the onset of coherence. Our results thus point to a coherence temperature of $\approx 45\ K$ for UBe_{13}, which is close to the maximum value found for T_{M2} (see Chapter 1) from resistivity measurements with the addition of Thorium impurities.

The frequency dependent mass enhancement was calculated using equation 3.4. It shows that as the frequency decreases the mass enhancement increases. This being more obvious as the temperature is decreased. At low temperatures, the mass enhancement is negative at high frequencies, crossing over to large positive values at low frequencies. At these temperatures a broad minimum is observed around 80 cm^{-1}. The low frequency enhancement at the lowest temperatures is ≈ 300 which is in good agreement with that determined from upper critical magnetic field measurements[21].

Appendix A

Reflectivity and Phase Shift

There are a number of ways to determine optical constants. A common way is to measure the reflectivity at normal incidence and use dispersion relations to determine the optical properties.

The reflectivity for normal incidence is given by:

$$R(\omega) = r(\omega)r^*(\omega) \tag{A.1}$$

where

$$r(\omega) = \frac{n - 1 + ik}{n + 1 + ik}. \tag{A.2}$$

We can write the complex reflectivity amplitude as

$$r(\omega) = \rho(\omega)e^{i\theta(\omega)} \tag{A.3}$$

where now

$$R(\omega) = \rho^2(\omega). \tag{A.4}$$

At first glance it would seem impossible to separate information about n and k from the reflectance measurements. It turns out however that one can overcome this difficulty by making use of a Kramers-Kronig dispersion relation which is an integral formula which relates a dispersive process to an absorption process.

Dispersion relations follow from the requirement of causality, i.e. that there can't be an effect before a cause.

Causality implies that absorption of one frequency must be compensated by a shift in phase, θ, of the other frequencies. The phase shift is given by the dispersion relation

$$\theta(\omega) = \frac{\omega}{\pi} \int \frac{ln(R(\omega')) - ln(R(\omega))}{\omega'^2 - \omega^2} d\omega' \tag{A.5}$$

Thus, if $R(\omega)$ is measured and $\theta(\omega)$ is determined via Equation A.5, then n and k can be obtained by solving Equations A.2 and A.3 in terms of $R(\omega)$ and $\theta(\omega)$.

$$n = \frac{1 - R}{1 + R - 2\sqrt{R}\cos\theta} \tag{A.6}$$

$$k = \frac{2\sqrt{R}\sin\theta}{1 + R - 2\sqrt{R}\cos\theta}. \tag{A.7}$$

Bibliography

[1] Z. Fisk, D. W. Hess, C. J. Pethick, D. Pines, J. L. Smith, J. D. Thompson, and J. O. Willis. Heavy-electron metals: New highly correlated states of matter. *Reprint Series*, 239:33, 1988.

[2] P. A. Lee, T. M. Rice, J. W. Serene, L. J. Sham, and J. W. Wilkins. Theories of heavy-fermion systems. *Comments Cond. Mat. Physics*, 12, Number 3:99-161, 1986.

[3] H. R. Ott. Ground-state properties of heavy electrons in u-intermetallics. *Physica B*, 130:163, 1985.

[4] C. Langhammer, R. Helfrich, A. Bach, F. Kromer, M. Lang, T. Michels, M. Deppe, F. Steglich, and G. R. Stewart. Evidence for the existence of two variants of UBe_{13}. *Journal of Magnetism and Magnetic Materials*, 177-181:443, 1998. *Physical Review B*, 54 No. 10:7401–7405, 1996.

[5] H. R. Ott and H. Rudigier. UBe_{13}: An unconventional actinide superconductor. *Physical Review Letters*, 50 No. 20:1595–1598, 1983.

[6] G. M. Schmiedeshoff, A. Lacerda, Z. Fisk, and J. L. Smith. Electrical resistivity of UBe_{13} in high magnetic fields. *Physical Review B*, 54 No. 10:7401–7405, 1996.

[7] F. Bommeli, L. Digiorgi, and P. Wachter. Possible non-fermi-liquid nature of paramagnetic UBe_{13}: The optical point of view. *Physical Review B*, 56 No. 16:R10001–10004, 1996.

[8] D. A. Bonn, R. J. Klassen, J. D. Garrett, and T. Timusk. Far infrared optical properties of heavy fermion superconductors UBe_{13} and URu_2Si_2. *Physica C*, 153-155:453–454, 1988.

[9] L. J. van der Pauw. A method of measuring specific resistivity and hall effect of discs of arbitrary shape. *Philips Research Report*, 13 No. 1:262–271, 1957.

[10] M. G. Hildebrand. *The Infrared Optical Properties of Sr_2RuO_4 and $SmTiO_3$ including an Object-Oriented Resistivity interface.* Brock University, St. Catharines, Ontario, 1999.

[11] A. Bajpai and A. Banerjee. An automated susceptometer for the measurement of linear and nonlinear magnetic ac susceptibility. *Rev. Sci. Instrum.*, 68:4075–4079, 1997.

[12] C. Kittel. *Introduction to Solid State Physics.* John Wiley and Sons, New York, 7th edition, 1975.

[13] W. Netchay. Brock university. Private comunication, Department of Physics, Brock University, 2000.

[14] A. Banerjee, A. K. Rastogi, M. Kumar, A. Das, and A. Mitra. Ac susceptibility apparatus for use with a closed cycle helium refrigerator. *J. Phys*, E22:231, 1989.

[15] G. Wardlaw. *Optical properties of MBe_{13} compounds from the MIR to the UV.* Brock University, St. Catharines, Ontario, 1999.

[16] Cryostat - Brock University Instruction manual. Infrared Laboratories.

[17] P. C. Eklund and et. al. Optical properties UBe_{13}, $CeBe_{13}$ and $ThBe_{13}$. *Physical Review B*, 35:4050, 1987.

[18] D. A. Bonn, J. D. Garrett, and T. Timusk. Far infrared properties of URu_2Si_2. *Physical Review Letters*, 61, Number 11:1305–1308, 1984.

[19] E. A. Knetsch, G. J. Nieuwenhuys, J. A. Mydosh, R. H. Heffner, and J. L. Smith. Normal state resistivity and specific heat of $U_{1-x}Th_xBe_{13}$. *Physica B*, 186-188:251–253, 1993.

[20] F. Wooten. *Optical Properties of Solids.* Academic Press, 111 Fifth Avenue, NY, NY 10003, 1972.

[21] M. B. Maple, J. W. Chen, and S. E. Lambert. Upper critical magnetic field of the heavy-fermion superconductor UBe_{13}. *Physical Review B*, 35:4050, 1987.

[22] S. Donovan, A. Schawartz, and G. Gruner. Observation of an optical psudogap in UPt_3. *Physical Review Letters*, 79, Number 7:1401–1405, 1997.

[23] S. V. Dordevic and D. N. Basov. Hybridization gap in heavy fermion compounds. *Physical Review Letters*, 86, Number 4:684–687, 2001.

[24] J. L. Smith, Z. Fisk, and J. O. Willis. Impurities in the heavy-fermion superconductor UBe_{13}. *J. Appl. Phys.*, 55:1996–2000, 1984.

[25] B. Mitrovic and P. N. Arberg. Optical conductivity of the Anderson impurity model. *Solid State Comunications*, 79:125–130, 1991.